Proceedings of the Canadian Society for Mechanical Engineering International Congress 2022
CSME Congress 2022
June 5-8, 2022, Edmonton, AB, Canada

ICE ACCRETION ON A ROTATING HORIZONTAL AXIS WIND TURBINE BLADE

Galal M. Ibrahim[1], Greg F. Naterer[2], Kevin Pope[3]
Department of Mechanical Engineering, Memorial University of Newfoundland, St. John's, NL, Canada
[1,*] gmi588@mun.ca, [2] gnaterer@mun.ca, [3] kpope@mun.ca

Abstract

This paper presents a numerical study of ice accretion on a 2 MW wind turbine with an 80 m rotor diameter using ANSYS FENSAP ICE software. The study investigates ice accumulaton with a focus on spanwise variability by analyzing four sections along a rotating blade. Air and droplet velocity contours, pressure distribution, droplet behavior, and ice characteristics are presented. The numerical results predict that radial distance towards the blade tip significantly impacts droplet collection and ice accretion. The results provide helpful insights for ice accretion modeling and mitigation along a blade span.

Keywords: Wind power, atmospheric icing, numerical predictions

I. INTRODUCTION

Wind turbines operating in high wind speeds and low temperatures are prone to severe ice loads [1]. For optimal wind turbine operation in cold regions, it is necessary to analyze changes in the air and droplet flow fields around the rotating blade during an icing event. Icing occurs due to the impingement of supercooled water droplets in the atmosphere, which freeze on the blade surface upon collision [2, 3]. Ice accretion on wind turbines depends on many variables including atmospheric conditions (e.g., pressure, temperature, droplet median diameter (MVD), and liquid water content (LWC)), operating conditions (e.g., wind speed, rotational speed, and tip speed ratio (TSR)), and blade design characteristics (e.g., roughness, material, airfoil, radius, and aerodynamic characteristics) [3].

Ice accretion on a wind turbine blade affects the flow behavior and degrades overall aerodynamic performance [4]. Its effects on wind turbine performance can be investigated using experimental and numerical approaches. Due to the large physical sizes, it is challenging to study icing on full-size wind turbines in a laboratory facility. Along with field measurements, computational fluid dynamics (CFD) simulations can be used to simulate, analyze and determine the performance of a wind turbine blade under icing conditions.

Past studies have shown significant power production loss due to ice occurring at sections near the blade tip [5-8]. Results indicated that the ice formation in terms of its local ice mass and accreted shapes are less severe near blade root sections, as characterized by larger and thicker blade profiles. Results showed that accreted ice growth changes significantly with the atmospheric temperature along the blade sections from the center to the tip [9]. In this paper, numerical simulations are performed to study the airflow and droplet behavior and predicted ice accretion on a large horizontal axis wind turbine using ANSYS FENSAP-ICE software.

II. METHODOLOGY

A. Two-phase flow and ice accretion modeling

Modeling of an icing event on a wind turbine blade is a complex process that involves airflow field simulations, water droplet trajectories, surface thermodynamics, and phase change computations. FENSAP [10] obtains airflow field solutions by solving partial differential equations for mass conservation, momentum, and energy. The Navier-Stokes equation in a relative frame of reference for a rotating blade is given by:

$$\rho_a\left[\frac{\partial\vec{V}_{r,a}}{\partial t}+\left[\vec{V}_{r,a}\cdot\nabla\right]\vec{V}_{r,a}\right]=\rho_a\vec{g}-\nabla p_a+\mu_a\nabla^2\vec{V}_{r,a}-\rho_a\vec{\Omega}\times$$

$$\left[\vec{\Omega}\times\vec{r}\right]-2\rho_a\left[\vec{\Omega}\times\vec{V}_{r,a}\right] \quad (1)$$

where ρ_a, μ_a, $V_{r,a}$, Ω, r, are air density, dynamic viscosity, air relative velocity, rotational speed, and distance from the axis of rotaion, respectively. DROP3D [10] predicts the two-phase flow using an Eulerian approach, consisting of the Navier-Stokes equations augmented with the droplet continuity and momentum equations [11]:

$$\alpha\left[\frac{\partial\vec{V}_{r,d}}{\partial t}+\left[\vec{V}_{r,d}\cdot\nabla\right]\vec{V}_{r,d}\right]=\frac{C_dRe_d}{24K}\alpha\left[\vec{V}_a-\vec{V}_d\right]+\alpha\left[1-\frac{\rho_a}{\rho_d}\right]\frac{1}{Fr^2}\vec{g}-$$

$$\alpha\vec{\Omega}\times\left[\vec{\Omega}\times\vec{r}\right]-2\alpha\left[\vec{\Omega}\times\vec{V}_{r,d}\right] \quad (2)$$

where α, $V_{r,d}$, Re_d, K, Fr, are the droplet's fraction, relative velocity, droplet Reynolds number, inertia parameter, and Froude number, respectively. This obtains droplet trajectories and collection efficiencies over the entire domain and blade surface. Local, β_o, and total, β, droplet collection efficiencies are defined as:

$$\beta_o=-\frac{\alpha\vec{V}_d\cdot\vec{n}}{LWC_\infty V_\infty} \qquad \beta=\frac{\int\beta_o dA}{A_{imp}} \quad (3)$$

where LWC_∞, A_{imp}, and n are the stream liquid water content, impingement area, and normal surface vector, respectively.

Finally, ICE3D [10] computes surface thermodynamics and predicts ice characteristics by modeling the mass transfer and heat fluxes generated due to supercooled water droplet impingement (i.e., source of the water film), evaporation, and ice accretion (i.e., sink of the water film). This leads to the ice accretion over the blade surface.

B. Computational domain and grid discretization

CFD grids are constructed at specific locations of interest along the blade sections to decrease the computational demands of testing at full-size. Four locations along the blade span are analyzed during an icing event. Boundary conditions (Fig. 1) for each grid include the flow inlet, exit, a non-slip blade wall, and symmetry. Each structured grid has a boundary layer thickness of 1×10^{-5} m up to 50 m with a growth rate of 1.15 over a NACA 4418 blade surface to avoid the wake region reverse flow and achieve a converged solution.

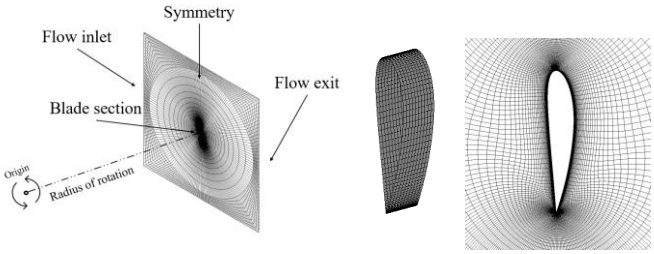

Figure 1. Discretization of the CFD domain and grid around blade airfoil

C. Numerical model setup and operating conditions

This study investigates ice accretion on a 2 MW power wind turbine model with an 80 m rotor diameter. An icing event is simulated using steady-state simulations for the flow field. A rotating frame of reference method is applied to each grid. Each blade section is set to rotate in the clockwise direction. A one-equation Spalart-Allmaras turbulence model is used to predict the turbulent flow around each rotating blade section. The Langmuir B [10] droplet model is used with seven droplet diameters ranging from 22 μm to 55 μm by computing the droplet concentration and speed for each droplet diameter of the discrete distribution and automatically determining an averaged solution at the end of the simulation. Four sections with a blade span of 0.5 m along the blade are tested for a specific icing condition. The blade design and configuration are based on the Blade Element Momentum (BEM) theory [12]. Fig. 2 shows velocity triangle discretization over a rotating blade and each tested section's pitch angle and chord to radius radio.

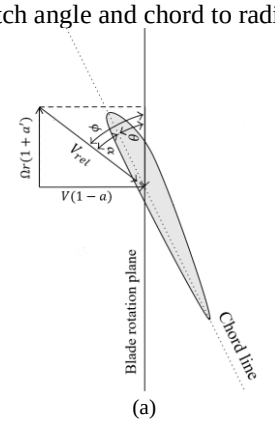

(a)

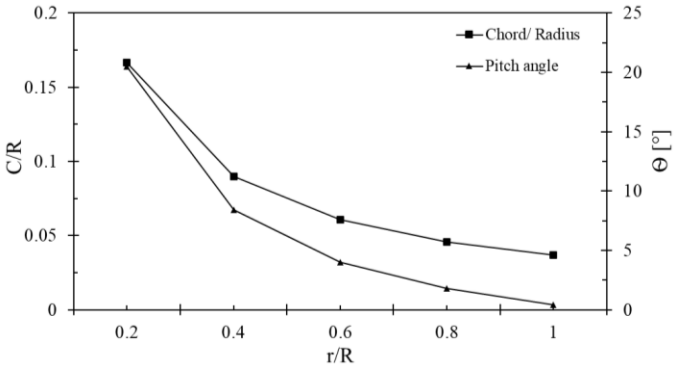

(b)

Figure 2. Velocity triangle with aerodynamic angle discretization (a) and 40 m radius blade - tested section design specifications (b)

The design process includes calculations for each blade section pitch angle, chord, angle of attack based on the optimal aerodynamic characteristics of a NACA 4418 airfoil at a specific Reynolds number of 10^6, and an optimal tip speed operation of 7. The blade origin point in XY plane is located at 30% of the chord line. The test section specifications are presented in Table 1. The operating conditions and icing event conditions are shown in Table 2.

TABLE 1. BLADE CHARACTERISTICS

Parameter	**Value**			
Angle of attack, α [°]	5			
Location, r/R	0.4	0.6	0.8	1
Chord, C [m]	3.59	2.43	1.84	1.47
Rotational radius, R [m]	16	24	32	40
Local speed ratio	2.8	4.2	5.6	7

TABLE 2. TEST CONDITIONS

Parameter	**Value**
Wind speed, V [m/s]	8.78
Rotational speed, Ω [RPM]	15
Icing temperature, T [°C]	-5
Droplet distribution – (size) [μm]	Langmuir B - (22 ~ 55)
Liquid water content, LWC [g/m^3]	0.5
Icing time, t [hrs]	3

III. RESULTS AND DISCUSSION

This section presents the results of the numerical predictions, including significant changes in the flow field (air and droplets) during an icing event on a wind turbine blade with NACA 4418 airfoil sections.

A. Air and droplet flow fields

Air velocity contours around the entire blade sections are obtained using the FENSAP solver. Air velocity contours with legends are presented in Fig. 3. Results show similar flow field behavior among different blade sections, from positions near the base (r/R = 0.4) to others near the tip (r/R = 1). However, higher velocity magnitudes exist over blade sections rotating at larger rotational distances of r/R (due to high relative speeds towards the tip).

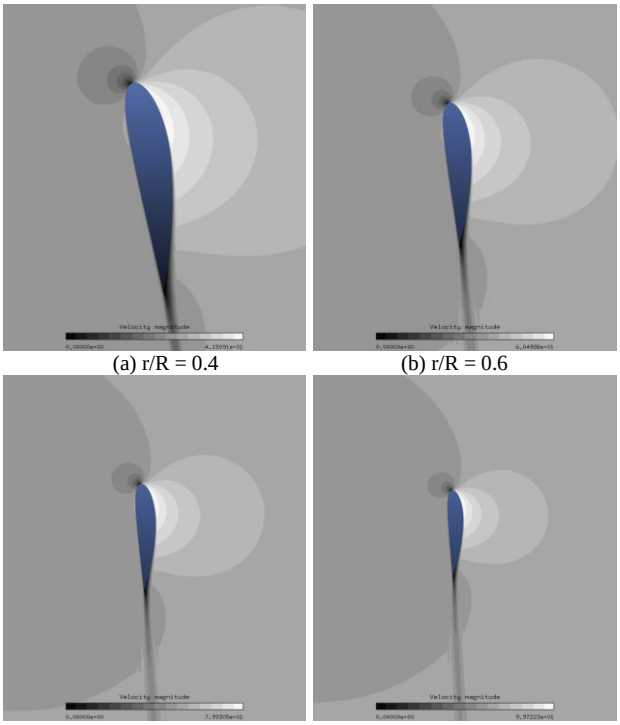

(a) r/R = 0.4 (b) r/R = 0.6

(c) r/R = 0.8 (d) r/R = 1

Figure 3. Airflow contours along blade span at different r/R ratios (R = 40 m)

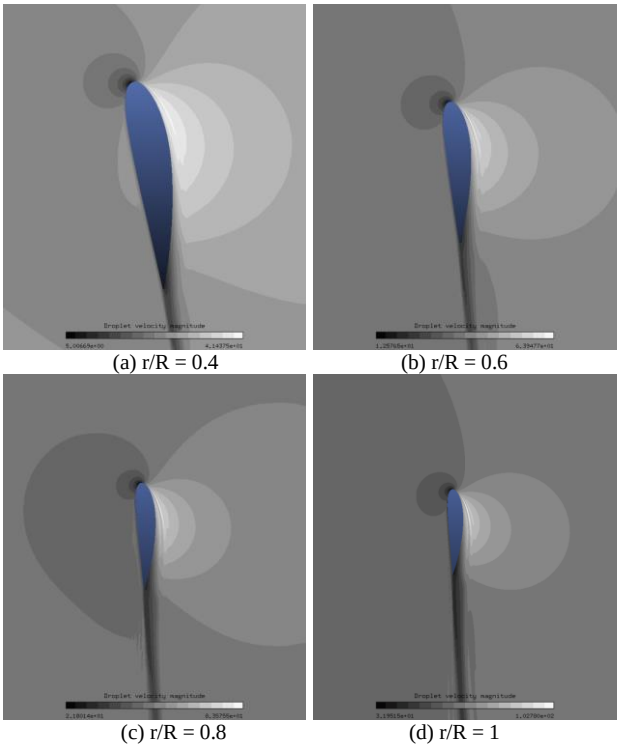

(a) r/R = 0.4 (b) r/R = 0.6

(c) r/R = 0.8 (d) r/R = 1

Figure 4. Droplet flow field contours along blade span at different r/R ratios (R = 40 m)

Droplet velocity contours around the entire blade sections are obtained using the DROP3D. As shown in Fig. 4, droplet velocity contours are similar to air velocity contours but have slightly different magnitudes. Results indicate that all droplets are in motion around the blade at a steady-state prior to the freezing process. Lower velocity magnitudes are found at the flow stagnation region.

B. Pressure distribution

Pressure coefficients over four different sections along the blade span are presented in Fig. 5. Results indicate slight changes in the pressure field due to each blade pitch angle variation. The right side represents the pressure side (positive values), and the left side represents the suction side (negative values). The pressure field significantly affects the aerodynamic characteristics. The results indiate these operating conditions and an optimal blade design could result in similar pressure fields along the blade span sections since sustained performance along the blade span is necessary.

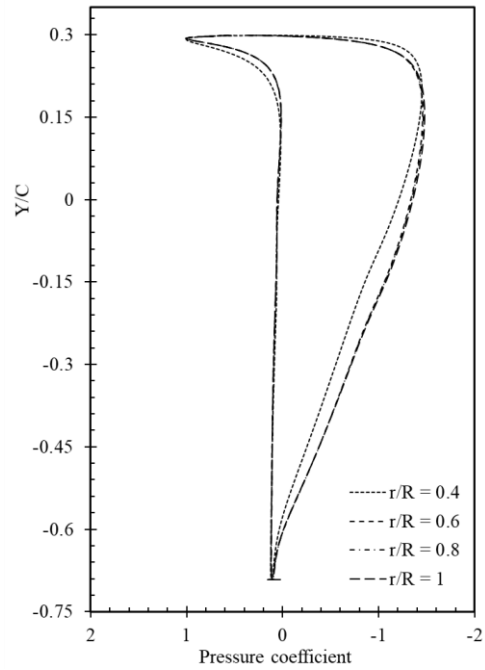

Figure 5. Pressure coefficients along blade span at different r/R ratios (R = 40 m)

C. Droplet impingement/collection

The DROP3D solver obtains droplet water volume fractions in kg/m^3 over the entire domain, including the blade surface. It uses droplet velocity magnitudes to compute local and total collection efficiencies. Fig. 6 shows droplet LWC contours over each blade section. Results indicate a hollow region with no droplet attachment towards the blade trailing edge, illustrating the droplet's collection at the leading edge. Fig. 7 shows local droplet LWC magnitudes along each blade section in the blade chordwise vertical direction Y/C and blade thickness-wise horizontal direction X/δ_{max} (δ_{max} is the maximum blade thickness). As shown in Figs. 7a and 7b., results indicate high droplet LWC values at the flow stagnation region (30% of chord length), with more area coverage for sections towards the blade tip.

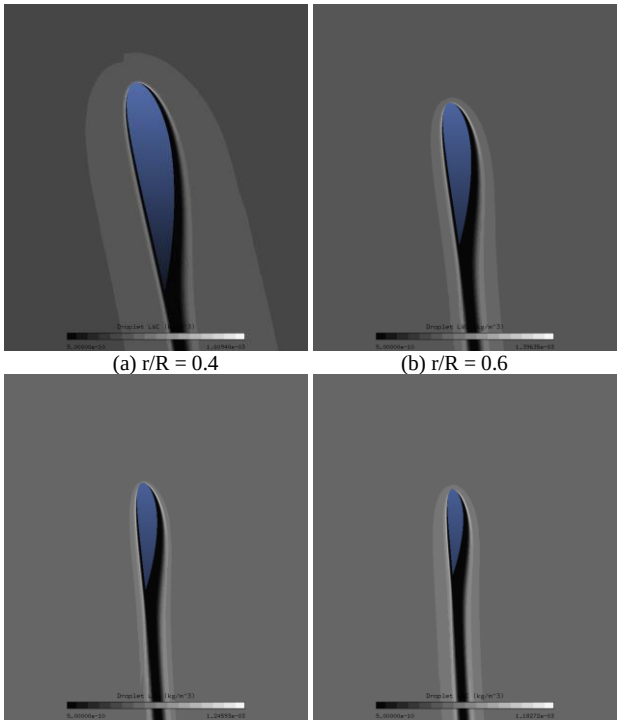

(a) r/R = 0.4 (b) r/R = 0.6

(c) r/R = 0.8 (d) r/R = 1

Figure 6. Droplet LWC contours along blade span at different r/R ratios (R = 40 m)

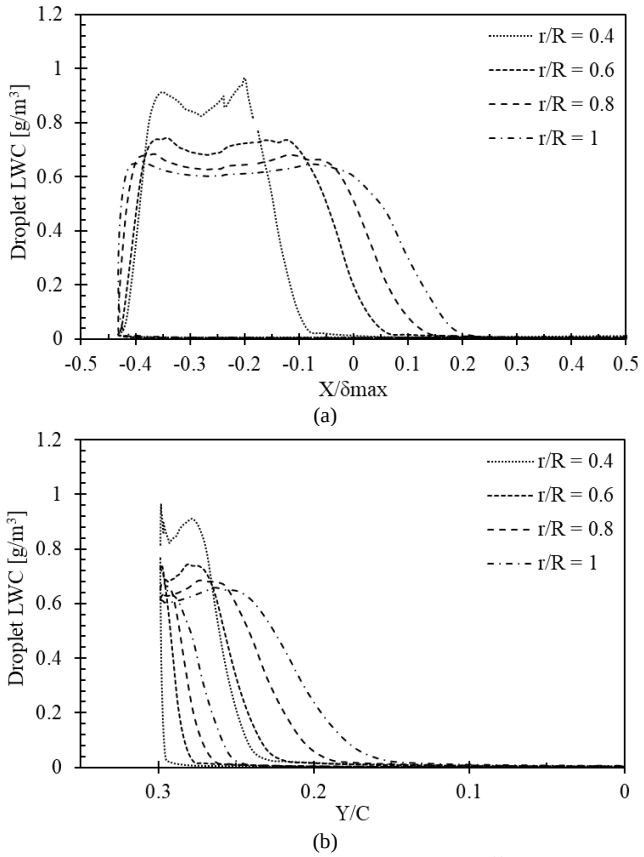

Figure 7. Droplet LWC distribution along blade span at different r/R ratios (R = 40 m) (a) X - direction and (b) Y - direction

Local droplet collection efficiency over a blade surface depends on the LWC fraction and droplet velocity at a location of interest. Integration of local collection efficiency values over a blade surface impingement area determines the total value for the collection efficiency. Fig. 8 shows local droplet collection efficiency values along the four-blade sections in X and Y directions. As shown in Figs. 8a and 8b, results indicate that more droplet collection and surface acquisition can occur at higher rotational distances towards the blade tip. Results indicates approximately 2.6 times increase in average collection efficiency value from sections at r/R = 0.4 to sections r/R = 1.

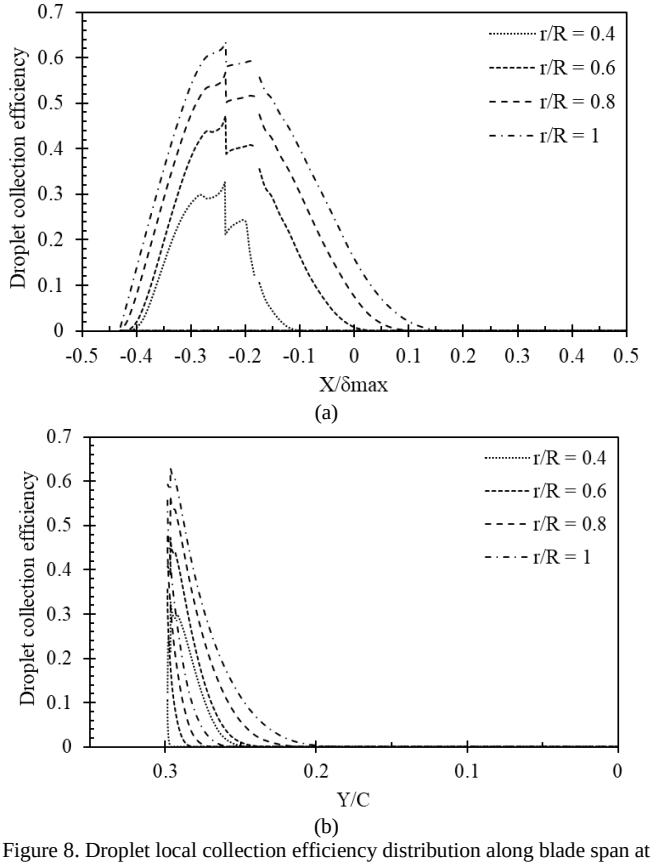

Figure 8. Droplet local collection efficiency distribution along blade span at different r/R ratios (R = 40 m), (a) X - direction and (b) Y - direction

D. Ice distribution and shape

The ICE3D solver predicts the ice formation caused by impinging droplets as a thin liquid water film on each solid surface. The film may run back when forced by the shear stresses created by the airflow, centrifugal forces, or gravitational forces. The height of the liquid film is to be determined at all grid points on the blade surfaces.

Based on the surface thermodynamic conditions, part of the water film may freeze, causing ice accretion, evaporation or sublimation. For comparison purposes, the local ice thickness distributions are presented for the different sections along the blade span in Figs. 9a and 9b. Results show that the maximum ice thickness can occur at the flow stagnation region, characterized by a high water collection efficiency. Results show a lower ice thickness at sections near the base than the tip, suggesting that ice horns are more likely to form on smaller

blade sections near the blade tip, as characterized by smaller chord lengths. Results indicates approximately 3.38 times increase in average ice thickness value from sections at r/R = 0.4 to sections r/R = 1.

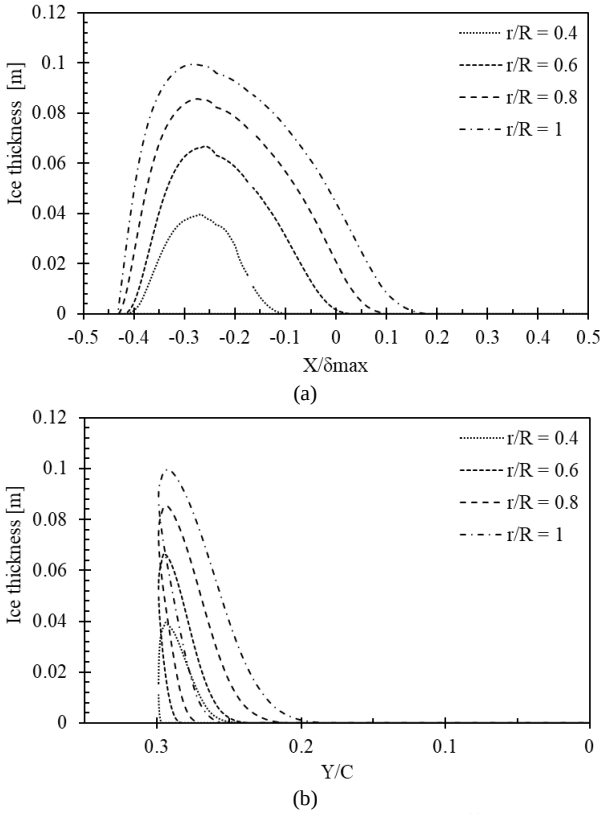

Figure 9. Ice thickness distribution along blade span at different r/R ratios (R = 40 m), (a) X - direction and (b) Y – direction

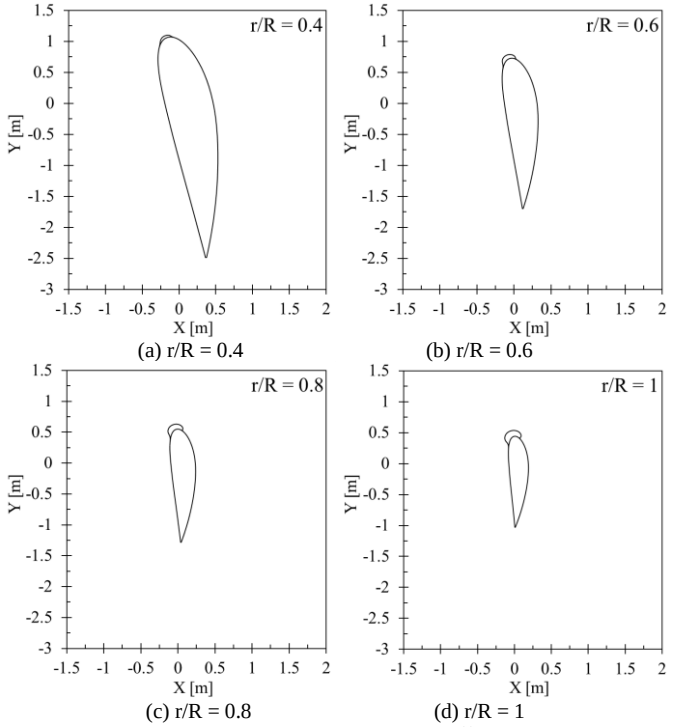

Figure 10. Predicted ice shapes along blade span at different r/R ratios (R = 40 m) (a) X - direction and (b) Y - direction

E. Effects of speed ratio

The speed ratio is a dimensionless parameter related to the efficiency and wind turbine blade design. Studies recommend an optimal value between 6 and 8 [13]. In this study, the blade model is designed at an optimal TSR value of 7, while ice is investigated at a specific icing condition. Predicted ice loads among different blade span sections are presented. The variation of ice quantity with the sectional speed ratio is shown in Fig. 9. Results show higher ice masses accumulate towards the blade tip than the blade root. Ice accretion in terms of mass and shape can be a critical problem for wind turbine blade sections near the tip.

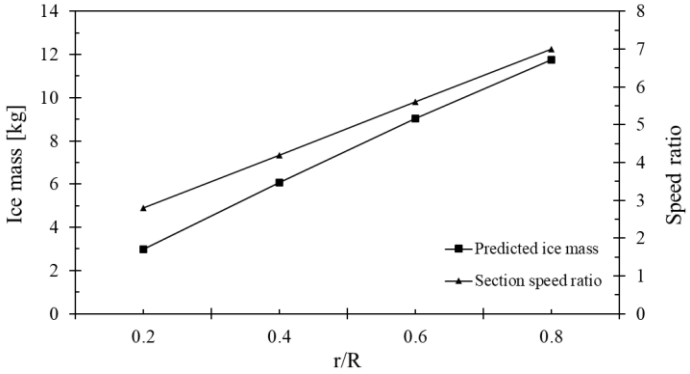

Figure 11. Predicted ice mass along blade span at different r/R ratios and sectional speed ratio

Local ice thickness values are used to predict ice shapes over the geometry. As shown in Fig. 10, results indicate comparatively large ice formations at later blade sections towards the blade tip. Results shows 3.95 times increase in ice mass at r/R = 1 when compared to ice at r/R = 0.4. This implies that ice accretion over areas near the blade tip can degrade the aerodynamic performance of a wind turbine blade.

IV. CONCLUSIONS

In this paper, ice accretion on a 2 MW power wind turbine blade model was investigated using FENSAP ICE. Four rotating sections on a 40 m radius wind blade located at 40%, 60%, 80%, 100% of its span were simulated during an icing event. The results indicated high droplet collection efficiencies at the leading edge of each blade section, especially at the flow stagnation point, with an increase of the value towards the blade tip by 2.6 times. Subsequently, larger ice thicknesses were mainly found at the blade's leading edge, with higher accumulations in terms of overall thickness by 3.38 times and mass by 3.95 times towards the tip sections. The results suggest higher ice loads are expected near the blade tip, contributing to aerodynamic losses in terms of overall lift and drag coefficients. The results provide useful insights for predicting ice accretion along a blade span at different configurations.

ACKNOWLEDGMENTS

The authors of this paper gratefully acknowledge the financial support of the Natural Sciences and Engineering Research Council of Canada (NSERC).

REFERENCES

[1] Jin, J. Y., Virk, M. S., Hu, Q., & Jiang, X. (2020). Study of ice accretion on horizontal axis wind turbine blade using 2D and 3D numerical approach. IEEE Access, 8, 166236-166245.

[2] Reid, T., Baruzzi, G., Ozcer, I., Switchenko, D., & Habashi, W. FENSAP-ICE simulation of icing on wind turbine blades, part 2: ice protection system design. In 51st AIAA Aerospace Sciences Meeting including the New Horizons Forum and Aerospace Exposition (p. 751), Grapevine, Texas, (2013).

[3] Battisti, L. (2015). Wind turbines in cold climates: Icing impacts and mitigation systems. Springer.

[4] Ibrahim, G. M., Pope, K., & Muzychka, Y. S. (2018). Effects of blade design on ice accretion for horizontal axis wind turbines. Journal of Wind Engineering and Industrial Aerodynamics, 173, 39-52.

[5] Han, W., Kim, J., & Kim, B. (2018). Study on correlation between wind turbine performance and ice accretion along a blade tip airfoil using CFD. Journal of Renewable and Sustainable Energy, 10(2), 023306.

[6] Han, Y., Palacios, J., & Schmitz, S. (2012). Scaled ice accretion experiments on a rotating wind turbine blade. Journal of Wind Engineering and Industrial Aerodynamics, 109, 55-67.

[7] Ibrahim, G. M., Pope, K., & Muzychka, Y. S. (2018). Transient atmospheric ice accretion on wind turbine blades. Wind Engineering, 42(6), 596-606.

[8] Yirtici, O., Ozgen, S., & Tuncer, I. H. (2019). Predictions of ice formations on wind turbine blades and power production losses due to icing. Wind Energy, 22(7), 945-958.

[9] Virk, M. S., Homola, M. C., & Nicklasson, P. J. (2012). Atmospheric icing on large wind turbine blades. Int. J. Energy Environ, 3(1), 1-8.

[10] ANSYS (2015) FENSAP-ICE User Manual R1.0, Canada

[11] Naterer, G. F., Advanced Heat Tranfer, 3rd Edition, CRC Press, Boca Raton, FL, 2022.

[12] Lanzafame, R. A., & Messina, M. (2007). Fluid dynamics wind turbine design: Critical analysis, optimization and application of BEM theory. Renewable energy, 32(14), 2291-2305.

[13] Cetin, N. S., Yurdusev, M. A., Ata, R., & Özdamar, A. (2005). Assessment of optimum tip speed ratio of wind turbines. Mathematical and Computational Applications, 10(1), 147-154.